Applied Physics A (2020) 126:303
https://doi.org/10.1007/s00339-020-03487-5

Applied Physics A
Materials Science & Processing

Investigation of the morphology, structural, optical, and photoelectrochemical properties of WO_3–Fe_2O_3/$CrTiO_2$ thin-film photoanodes for water splitting

Mohamad Mohsen Momeni[1] · Yousef Ghayeb[1] · Farzaneh Ezati[1]

Received: 13 November 2019 / Accepted: 23 March 2020 / Published online: 30 March 2020

Abstract
$CrTiO_2$ nanotube, tungsten-modified $CrTiO_2$, iron-modified $CrTiO_2$ and tungsten–iron-modified $CrTiO_2$ have been prepared by facile one-step anodization coupled with chemical bath deposition method. XRD, FE-SEM, EDX mapping and UV–Vis spectroscopy were used to characterize the synthetic samples. The impacts of these compounds on the photoelectrochemical activities of modified $CrTiO_2$ photoelectrodes have been studied. Photoelectrochemical (PEC) water splitting performance of bare $CrTiO_2$ nanotube photoelectrodes has remarkably been increased by hybrid tungsten–iron–$CrTiO_2$ nanotube composite photoelectrodes. Good photoelectrocatalytic and stable photoelectrochemical performance have been shown by tungsten–iron–$CrTiO_2$ (denoted as S6). The synergistic effect of WO_3, Fe_2O_3 and $CrTiO_2$ can be accounted for the considerable increase in the performance of tungsten–iron-modified $CrTiO_2$, enhancement of optical absorption in the visible region and the suitable band positions of these composites. Ultimately, the recyclability of the synthetic tungsten–iron-modified $CrTiO_2$ photocatalysts showed the good stability of their photocatalytic activity.

Keywords $CrTiO_2$ nanotube · Tungsten · Iron · Photoelectrode · Photoelectrocatalysis · Photoelectrochemical water splitting

1 Introduction

The development of clean energy sources is very vital to overcome the present environmental problems and assure sustainability. Since it was first reported by Fujishima, photoelectrochemical (PEC) water splitting has shown to be a renewable energy conversion technique [1]. Different metal oxide semiconductors such as SnO_2, CeO_2, CuO, Cu_2O, Ta_2O_5, TiO_2, ZnO, Fe_2O_3 and WO_3 and the corresponding composites have been extensively used as photoelectrodes (photoanodes or photocathodes) in photoelectrochemical cells [2–9]. One of such oxides is titanium oxide (TiO_2), which has been known as an outstanding candidate photoanode in photoelectrochemical water splitting cells given its strong oxidation resistance, abundance, good stability, low cost, low toxicity, remarkable photostability and efficient photoelectrocatalytic performance [6, 9]. One-dimensional TiO_2 nanostructures, especially TiO_2 nanotubes, have been of considerable interest because of their geometrical shape, optical and electrical characteristics. The TiO_2 nanotube vertical nature gives rise to good charge transfer between interfaces and large internal surface area while not decreasing the geometric and structural order. Nanotube structures have reportedly facilitated the separation of the photo excited charges, promoting high charge collection efficiencies compared with ordinary TiO_2 nanostructures [9–11]. In addition, it must be indicated that TiO_2 nanotubes increase the light absorption and propagation since photons enter these nanotubes. Therefore, they are very unlikely to escape due to multiple radiations scattering through the walls. Two factors, however, restrict the practical application of pure TiO_2 photoanode [9–11]:

(1) Wide band gap (TiO_2 only performs under UV light irradiation with a wavelength below 387 nm. This only

Electronic supplementary material The online version of this article (https://doi.org/10.1007/s00339-020-03487-5) contains supplementary material, which is available to authorized users.

✉ Mohamad Mohsen Momeni
mm.momeni@cc.iut.ac.ir

[1] Department of Chemistry, Isfahan University of Technology, Isfahan 84156-83111, Iran

covers 4% of the solar spectrum and greatly impedes its photocatalytic applications in the visible light range)

(2) The short minority carrier (hole) diffusion length and the low electron mobility, both of which limit TiO_2 quantum efficiency.

Different strategies have been developed to extend light absorption properties and improved visible light photocatalytic activity of TiO_2. Some most-used strategies are doping of TiO_2 with metal and non-metal, surface modification of TiO_2 nanostructures and preparation of heterojunction composites based on TiO_2 [8–11]. A facile and novel method for co-deposition of tungsten–iron on the $CrTiO_2$ nanotube surfaces is reported. This process consists of two steps: (1) preparation of highly ordered $CrTiO_2$ nanotubes by a facile single-step anodization method; (2) deposition of tungsten–iron on the nanotube surfaces by chemical bath deposition (CBD) process. Amount and ratio effects of these nanoparticles on the PEC activity of these samples have been studied. An effective area to receive light and vast active sites for electrons are provided by this composite due to the large surface area of $CrTiO_2$ nanotubes. The combined large surface area of nanotubes and photocatalytic activity of tungsten oxide–iron oxide may improve charge separation and stabilization. Tungsten oxide (WO_3) is a narrow band gap semiconductor (2.4–2.8 eV) and can absorb light in the visible region of the solar spectrum. In addition, because of its low cost, harmlessness, and stability in acidic and oxidative conditions and also its good charge-carrier transport properties, WO_3 is a very attractive semiconductor for photocatalytic and photoelectrochemical applications [12, 13]. Hematite (α-Fe_2O_3) is an *n*-type semiconductor and one of the best candidates for photocatalytic applications. Because of appropriate band gap (2.1 eV) for the absorption of visible light, stability in most aqueous solutions (except in strongly acid conditions), non-toxicity, high availability, low cost, and excellent photoelectrochemical, hematite has been considered a promising metal oxide semiconductor for photocatalytic applications [14]. Recently our research groups have focused on improving the performance of TiO_2-based photocatalytic materials supported on titanium substrate by co-doping or simultaneous deposition of two metal oxides to obtain heterojunction systems with high photocatalytic activity and good stability. The preparation of tungsten–iron co-deposited $CrTiO_2$ nanotube composite photoelectrodes by chemical bath deposition and anodization processes and application of these compounds in photoelectrochemical water splitting has not yet been studied.

2 Experimental

2.1 Fabrication of tungsten–iron co-deposited $CrTiO_2$ nanotube photoelectrodes

$CrTiO_2$ nanotubes on Ti foils were first prepared by the electrochemical anodization method. 0.25-mm-thick Ti foils of over 99.9% purity were used in this previously reported method [11]. A constant voltage of 60 V was applied in the anodization over a period of 6 h. The surface debris and residual electrolyte were rinsed off the obtained $CrTiO_2$ nanotube/Ti substrates using distilled water, and the product was then air-dried. CBD method was applied to prepare the tungsten–iron co-deposited $CrTiO_2$ nanotubes in the second step. $CrTiO_2$/Ti samples were soaked in 0.1 M H_2SO_4 solution for 1.5 h and aqueous solution of $Na_2WO_4{\cdot}2H_2O$ and $FeCl_3{\cdot}6H_2O$ for 0.5 h at 70 °C subsequently. The product was then rinsed with distilled water and air-dried. To form metal oxides and obtain crystalline samples, the samples were then annealed by heating at 400 °C for 2 h at a rate of 2 °C/min. The photoelectrochemical activity of $CrTiO_2$ and $CrTiO_2$ nanotubes co-deposited using various tungsten/iron ratios, namely S0, S1, S2, S3, S4, S5, S6 and S7, have been compared in this work. Figure 1 shows a schematic representation for the preparation of tungsten–iron co-deposited $CrTiO_2$ films on Ti foil. Also the experimental conditions for the preparation of different co-deposited $CrTiO_2$ nanotube samples are given in Table 1.

2.2 Material characterization and electrochemical measurements

X-ray diffraction (XRD, Philips X'Pert PRO, Cu-Ka radiation) patterns were used to study the crystal structure of prepared materials. Field emission scanning electron microscopy (FE-SEM, Hitachi S-4160, Japan) was used to study the surface morphology of the nanostructures. The measurement of the absorption of prepared electrodes and estimation of their band gap values was carried out by UV–Vis spectroscopy. A UV–Vis spectrophotometer (JASCO V-570) in the range of 250–600 nm was used for this purpose. An Origaflex electrochemical working station (OGF500 potentiostat/galvanostat, France) was used to perform the photoelectrochemical measurements. PEC experiments were carried out using a standard three electrode electrochemical system. A photoanode (area = 1 cm^2), an Ag/AgCl/saturated KCl electrode and a Pt foil were applied as the working, reference, and counter electrodes, respectively. To measure the photocurrent, the photoanodes were immersed in a 1 M KOH solution (pH 13.6). A 35 W xenon lamp with a luminous intensity of

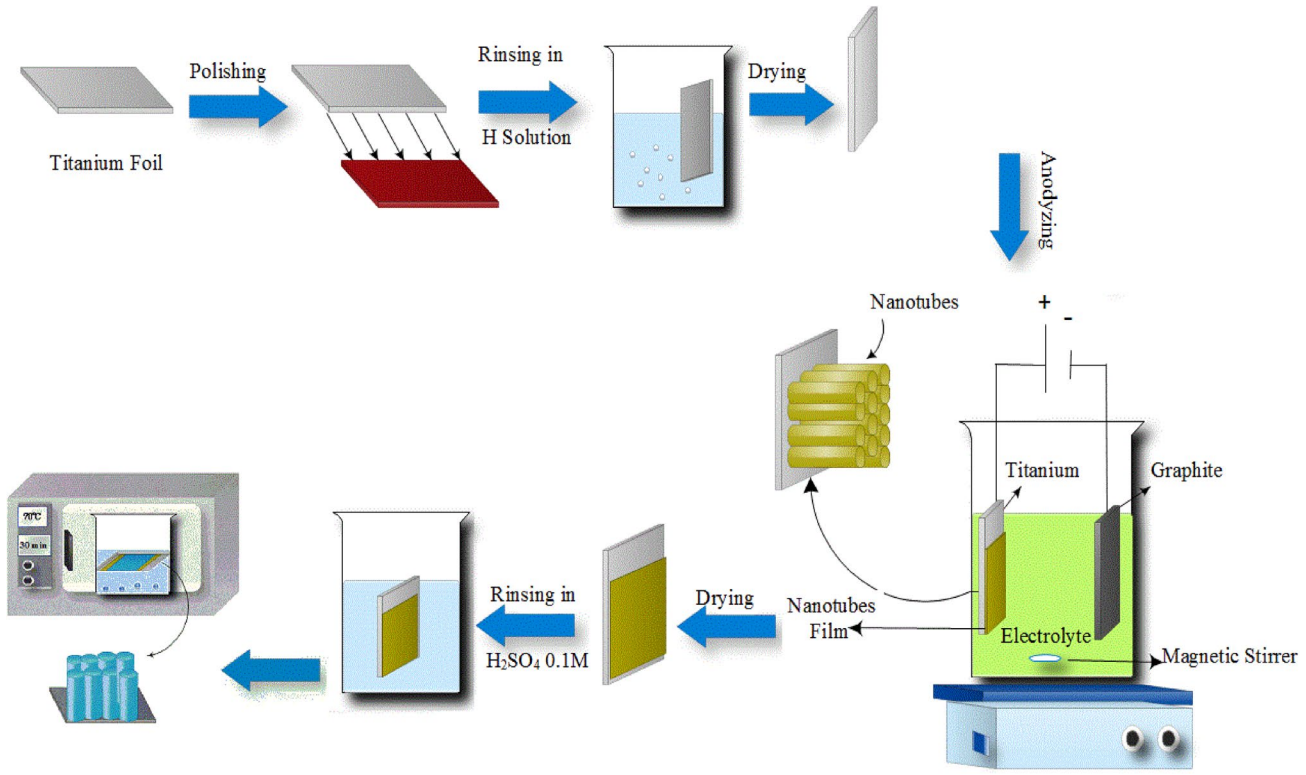

Fig. 1 Schematic preparation process of W–Fe-modified $CrTiO_2$ nanotube on Ti foils

Table 1 The experimental parameters for the synthesis of samples (anodization of titanium were performed in a solution of ethylene glycol. (98 ml) containing 0.1 M ammonium fluoride, 5 mM potassium chromate and 2 ml distilled water at 60 V for 6 h)

Samples	Chemical bath deposition for 30 min at 70 °C in aqueous solution (3:1 $C_2O_4^{2-}$:Fe^{3+}) containing following composition
S0	–
S1	0.10 M $Na_2WO_4{\cdot}2H_2O$
S2	0.08 M $Na_2WO_4{\cdot}2H_2O$ + 0.02 M $FeCl_3{\cdot}6H_2O$
S3	0.060 M $Na_2WO_4{\cdot}2H_2O$ + 0.04 M $FeCl_3{\cdot}6H_2O$
S4	0.05 M $Na_2WO_4{\cdot}2H_2O$ + 0.05 M $FeCl_3{\cdot}6H_2O$
S5	0.04 M $Na_2WO_4{\cdot}2H_2O$ + 0.06 M $FeCl_3{\cdot}6H_2O$
S6	0.02 M $Na_2WO_4{\cdot}2H_2O$ + 0.08 M $FeCl_3{\cdot}6H_2O$
S7	0.10 M $FeCl_3{\cdot}6H_2O$

200 mW/cm was used to illuminate the obtained electrodes with an approximately 1 cm^2 area[2].

3 Results and discussion

SEM images of $CrTiO_2$ sample showed the formation of vertically ordered nanotube arrays on the titanium substrate surface. These samples were found to consist of a layer of tubes. The tube inner diameter is around 70–120 nm [11]. The FE-SEM images of different co-deposited $CrTiO_2$ nanotubes are shown in Fig. 2. As observed, the nanotubular structure of $CrTiO_2$ has maintained its integrity with no significant morphological change following co-deposition. It can be seen that nanoparticles were deposited on the nanotube surfaces via CBD process. Increasing iron concentration in CBD solution causes the deposition of more nanoparticles on the $CrTiO_2$ nanotubes and the agglomeration of deposited nanoparticles at the top of the nanotubes, blocking the nanotubular structures (sample S7). This is undesirable and reduces the nanotube specific surface area and thus decreases the performance of these samples, as indicated in the photoelectrochemical test part.

XRD was used to characterize prepared electrodes. The crystalline nanotube shows an anatase structure for TiO_2 (JCPDS No.73-1764), as observed in Fig. 3. Some peaks are observed for Cr_2O_3 in the XRD pattern of tungsten–iron co-deposited $CrTiO_2$ samples. This can be indexed to those of pure rhombohedral phase Cr_2O_3 (JCPDS No. 38-1479). The Ti peaks were associated with the titanium substrate. Furthermore, the diffraction peaks of Fe_2O_3, WO_3 and TiO_2 are shown in the XRD pattern of co-deposited $CrTiO_2$. The diffraction peaks ($2\theta = 27°$, 48°, 54°, 55°, 76° and 77°) are ascribed to the reflections corresponding to the tungsten oxide (WO_3) phase, a monoclinic

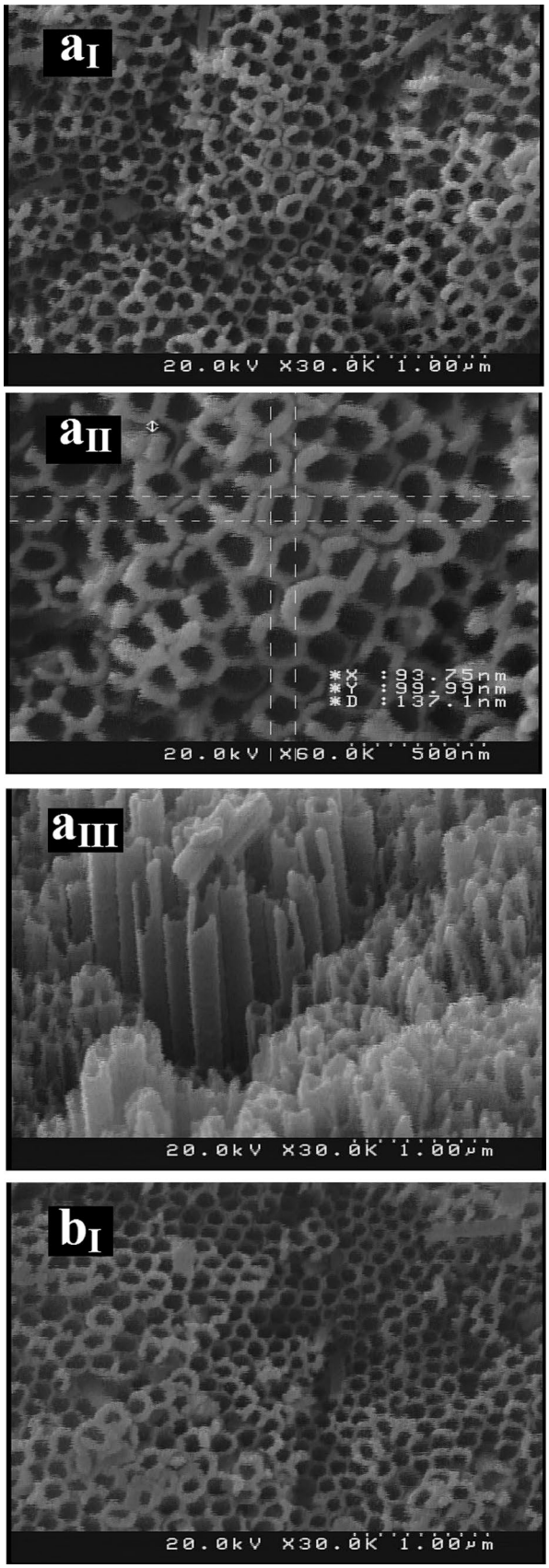

Fig. 2 SEM images of different W–Fe-modified $CrTiO_2$ samples; **a** ▶ S1, **b** S2, **c** S3, **d** S4, **e** S5, **f** S6 and **g** S7

crystal system (JCPDS data file 72-1465). Clear diffraction peaks corresponding to Fe_2O_3 are observed in the XRD pattern of the co-deposited $CrTiO_2$ nanotubes. All the peaks in the XRD patterns are clearly observed to be consistent with the JCPDS data (No. 39-1346) of Fe_2O_3. No detectable diffraction peaks due to the possible impurities are observed, suggesting the high product purity. In addition, the content of the Fe_2O_3 peaks increases as the amount of iron in CBD solution increases. EDX mapping was used to confirm the composition of tungsten–iron co-deposited $CrTiO_2$ nanotubes (Figures S1 and S2). The presence of W, Fe, Cr, Ti, O, Na, F and N is shown by these tests in the samples. W, Cr, Ti, and Fe were homogeneously distributed on the sample surfaces, as indicated by the elemental maps.

The optical properties of the synthetic samples were studied, and obtained results are shown in Figure S3. The samples showed enhanced absorption in the visible light range upon loading of tungsten and iron on the $CrTiO_2$ nanotubes. The band gaps were investigated for further investigation of the band gap change of the co-deposited $CrTiO_2$ samples. The Tauc plot and the equation represented below can be used to quantitatively determine the optical band gap:

$$(\alpha h\upsilon) = A\left(h\upsilon - E_g\right)^n \quad (1)$$

where α, h, υ, A and n are the absorption coefficient, the Plank's constant (6.6260×10^{-34} J s), the radiation frequency, a constant and a number characterizing the transition, respectively [11, 15, 16]. The relationship between $(\alpha h\upsilon)^{0.5}$ and $h\upsilon$ of different co-deposited $CrTiO_2$ nanotubes is shown in Figure S3. The band gap value was about 2.2–2.6 eV for the tungsten–iron co-deposited $CrTiO_2$ samples because of loading of Fe_2O_3 and WO_3. This caused the reduction of the band gap value, thus showing the visible light activity of these new samples.

Linear sweep voltammograms were used to investigate the photoelectrochemical activities of the samples (Figures S4). The dark current from -0.5 to $+1$ V (vs. Ag/AgCl) of all electrodes was almost zero as a result of inactivation of electron hole phenomenon. Upon exposure of these electrodes to light, they show significantly enhanced photocurrent response because of the triggering of photo induced electron hole pair separation. The photoelectrochemical current response of all the deposited $CrTiO_2$ samples shows an important increase (also see Figure S5) compared with the bare $CrTiO_2$.

Figure 4a shows the J–V curves for different samples under light chopping. The observed dark current density

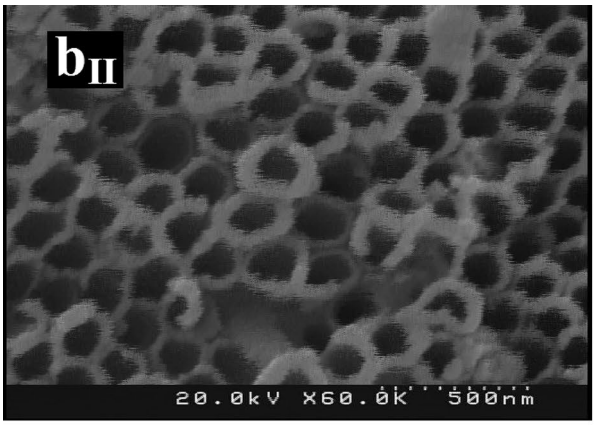

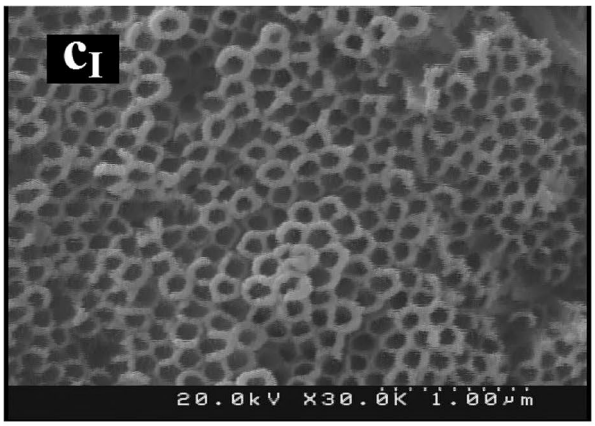

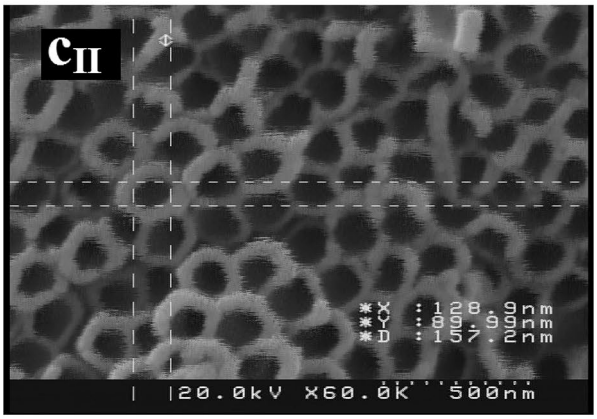

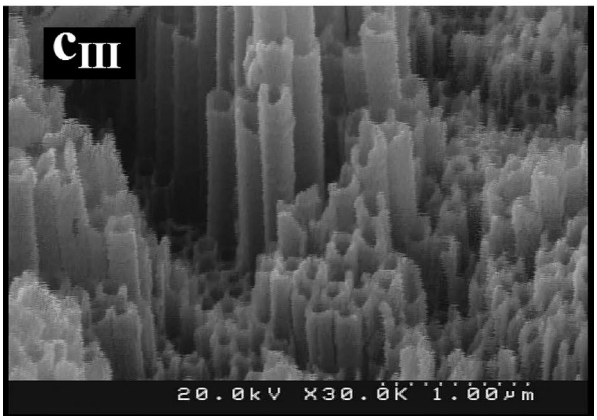

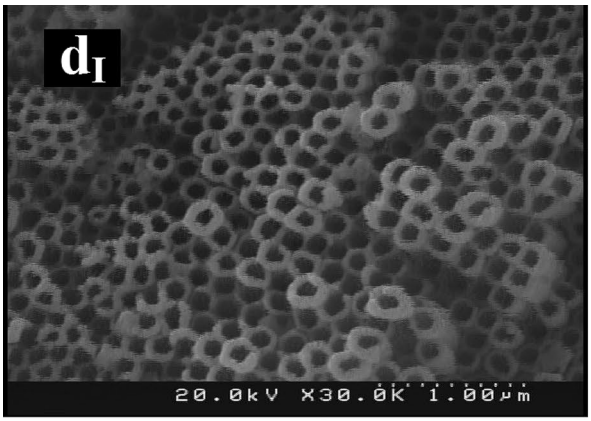

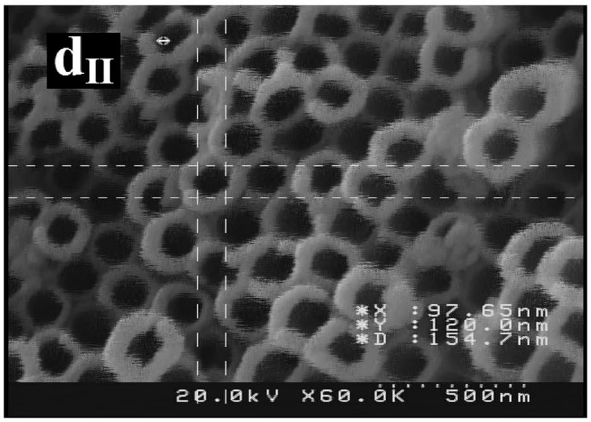

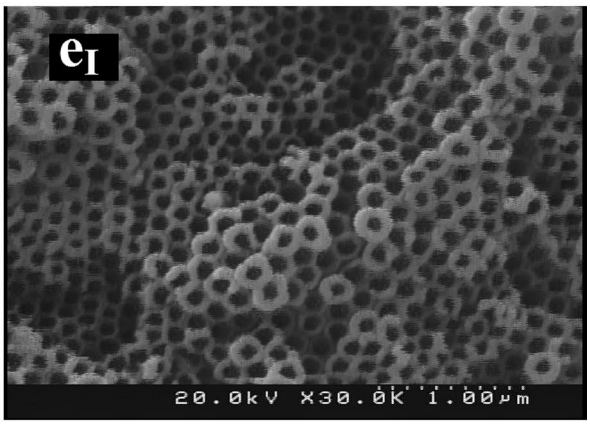

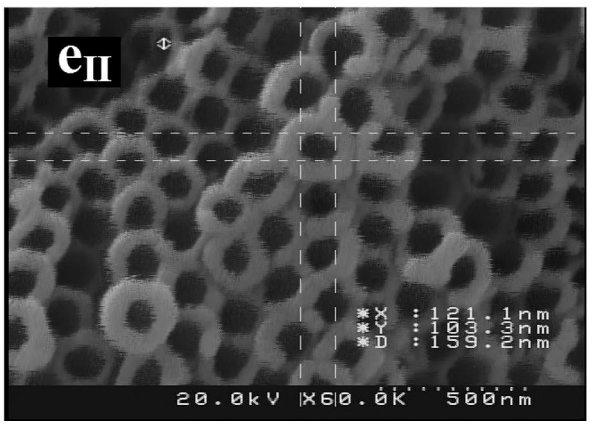

Fig. 2 (continued)

Fig. 2 (continued)

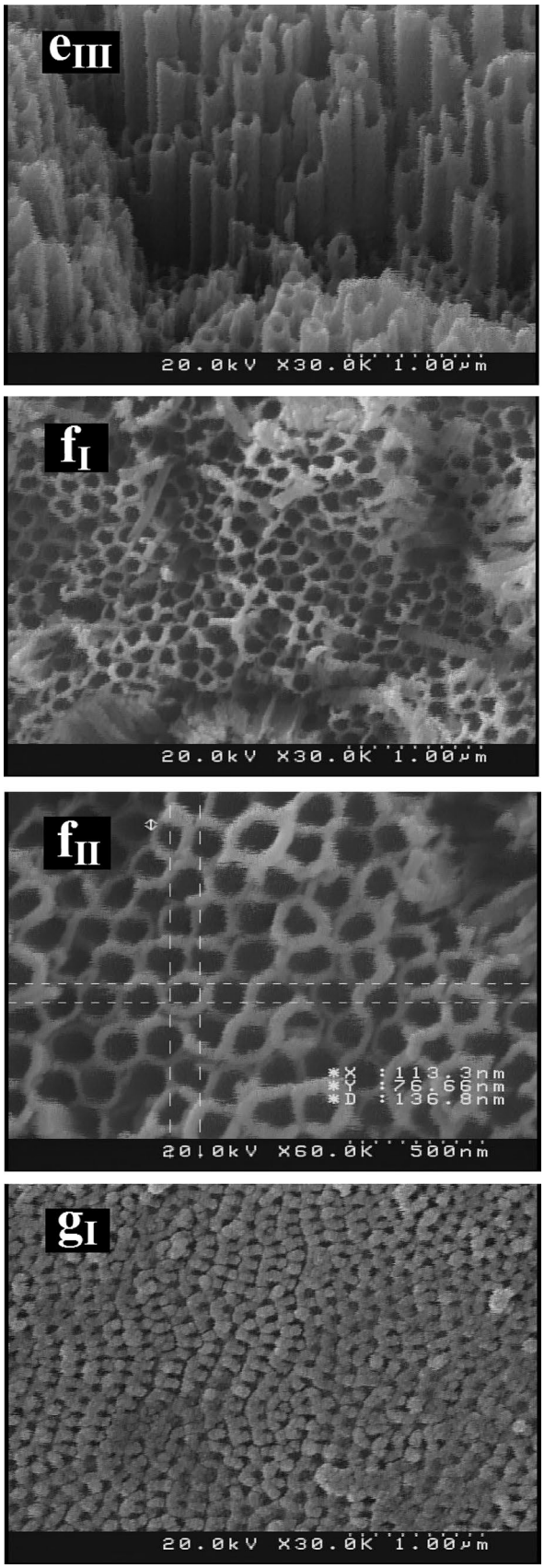

Fig. 2 (continued)

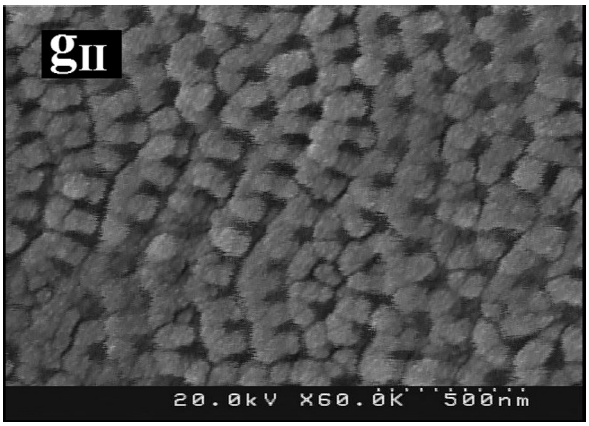

Fig. 2 (continued)

was negligible for all electrodes. The current density of each electrode, however, is completely different under illumination. Tungsten–iron co-deposited $CrTiO_2$ photoanodes exhibited improved photocurrent densities in comparison with bare $CrTiO_2$, according to Fig. 4a. The photocurrent density of bare $CrTiO_2$ (sample S0) was found to be 126 $\mu A/cm^2$ at +0.6 V versus Ag/AgCl. However, the highest photocurrent densities of 918 $\mu A/cm^2$ by sample S6 and significant photocurrents were measured for samples following tungsten–iron co-deposition. Samples S7, S6, S5, S4, S3, S2, S1 and S0 had photocurrents of 206, 918, 376, 351, 557, 655, 276 and 126 $\mu A/cm^2$, respectively (Fig. 4a). Higher photocatalytic activity was shown by $CrTiO_2$ nanotube co-deposited with tungsten–iron binary nanoparticles compared with the $CrTiO_2$ nanotube deposited with just tungsten or iron nanoparticles. This indicates the strong synergistic effect of the three materials (chromium, tungsten and iron). In addition, molar ratios of tungsten–iron in chemical bath deposition solutions play a significant part in the photocatalytic performance.

The measurements of the rise and fall of the photocurrent during on–off cycles under light irradiation are also observed in Fig. 4b. No current was in the dark and the photocurrent reached the steady state when a sharp current spike was formed under light irradiation, according to the figure, indicating that the prepared samples exhibited good photoelectrochemical performance. Photocurrent density-time curves clearly show that the photocurrent density increases with co-deposition of tungsten–iron on the $CrTiO_2$ nanotubular samples. All the curves remain steady without any decay throughout the measurement period. Moreover, a correlation exists between the coating composition, namely the molar ratios of tungsten–iron in chemical bath deposition solution, morphology and the photocurrent density increase. In addition,

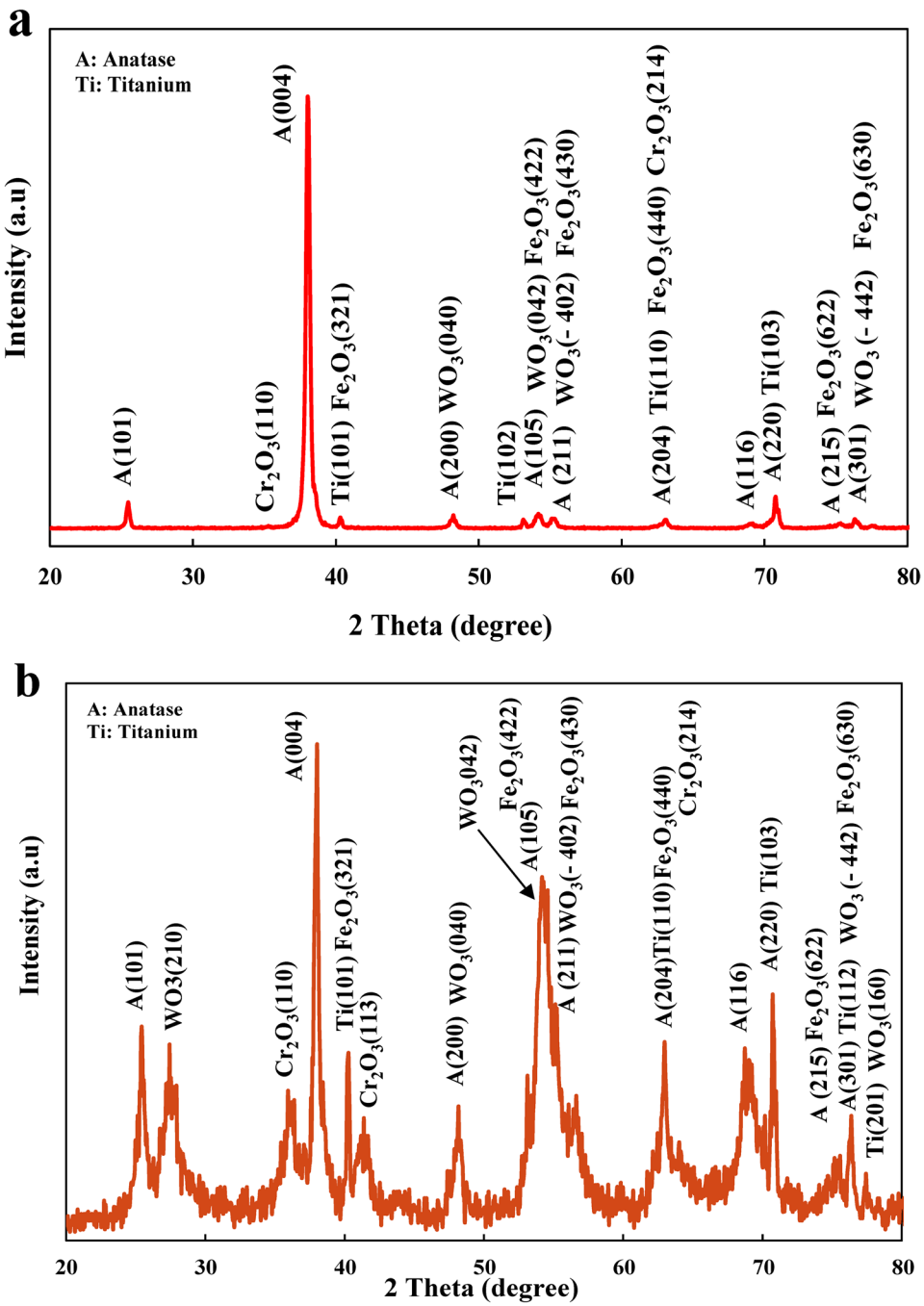

Fig. 3 XRD patterns of different samples annealed at 400 °C; **a** S2 and **b** S6

the photocurrent stability of these samples was evaluated for 1200 s at + 0.60 V versus Ag/AgCl in 1 M KOH with the addition of 5 vol% ethylene glycol to study the photocatalytic chemical stability of the prepared nanotubular photoanodes. As Fig. 4c shows, the photocurrent density of the prepared samples does not decrease and the samples maintain their high photocatalytic activity for a long period of time (also see Figure S6). Equation 2 is used to calculate the solar-to-chemical conversion efficiency (η):

$$\eta(\%) = \left[(\text{total power output} - \text{electrical power input})/\text{light power input}\right] \times 100$$
$$= \left[I\,(1.23 - |E_{\text{app}}|)/J_{\text{light}}\right] \times 100$$

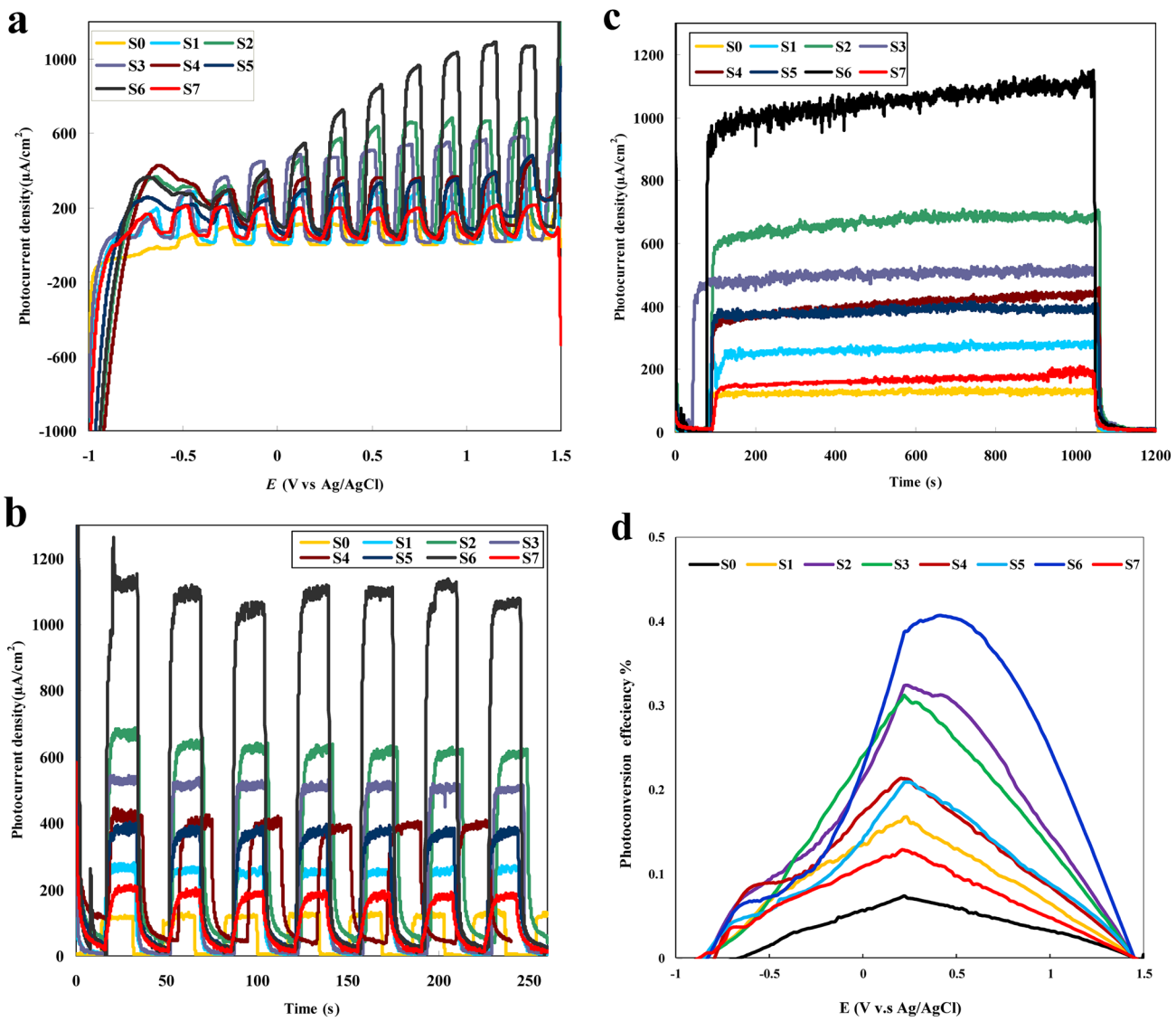

Fig. 4 **a** Current potential curve of different samples under chopped light in 1 M KOH solution (pH 13.6) with the addition of 5 vol% EG and a scan rate of 10 mV s^{-1}. **b** Transient photocurrent characteristics ($I_{ph} - t$) of different nanocomposites under illumination at +0.6 V versus Ag/AgCl electrode. **c** Photocurrent density stability for longer period of time at a bias potential of 0.6 V (vs. Ag/AgCl) for different samples. **d** Optical-to-chemical conversion efficiency of different photoanodes under the xenon lamp illumination

where I, E_{app} and J_{light} are the externally measured photocurrent density, applied potential versus reversible hydrogen electrode (RHE) and irradiance intensity, respectively. The applied potential (E_{app}) is defined as the difference between the electrical potential (vs. Ag/AgCl) of the working electrode under illumination (E_{meas}) and the same electrode under open circuit conditions (E_{aoc}) [16]. The corresponding η values for S0, S1, S2, S3, S4, S5, S6 and S7 samples under 200 mW cm^{-2} illumination are ~ 0.07, 0.16, 0.32, 0.31, 0.21, 0.20, 0.41 and 0.13%, respectively (Fig. 4d). Consequently, $CrTiO_2$ nanotubes co-sensitized with tungsten–copper such as sample S6 can increase the maximum photocurrent over 5 times in comparison with bare $CrTiO_2$ nanotubes and greatly enhance the efficiency of photoconversion.

4 Conclusion

The following are the major conclusions from this work:

- Preparation of $CrTiO_2$ nanotubes by facile one-step anodization.
- Potassium chromate was used as the chromium source in the anodization process.

- Successful synthesis of tungsten and iron co-deposited $CrTiO_2$ nanotubes by CBD.
- Characterization of the synthetic samples by FE-SEM, XRD, EDX mapping and UV–Vis techniques.
- The presence of chromium, tungsten and iron in these samples, as shown by XRD and EDX mapping analyses.
- Systematic investigation of the effects of the amount and ratio of W and Fe on the PEC water splitting performance of the samples.
- Stability of the photoelectrodes for repeated use.
- Proposing a promising practical application of non-noble metals as co-catalysts for PEC water splitting into hydrogen.

References

1. A. Fujishima, K. Honda, Electrochemical photolysis of water at a semiconductor electrode. Nature **238**, 37–38 (1972)
2. J. Zhang, H. Ma, Z. Liu, Highly efficient photocatalyst based on all oxides WO_3/Cu_2O heterojunction for photoelectrochemical water splitting. Appl. Catal. B **201**, 84–91 (2017)
3. Z. Zhang, C. Gao, Y. Li, W. Han, W. Fu, Y. He, E. Xie, Enhanced charge separation and transfer through Fe_2O_3/ITO nanowire arrays wrapped with reduced graphene oxide for water-splitting. Nano Energy **30**, 892–899 (2016)
4. J.H. Seo, G. Park, K.H. Oh, S.H. Kang, H.C. Lee, S.K. Cho, K.M. Nam, Analysis of charge separation processes in WO_3–$BiVO_4$ composite for efficient photoelectrochemical water oxidation. J. Electroanal. Chem. **789**, 17–23 (2017)
5. Y.F. Su, M.C. Lee, G.B. Wang, Y.H. Shih, An innovative method to quickly and simply prepared TiO_2 nanorod arrays and improve their performance in photo water splitting. Chem. Eng. J. **253**, 274–280 (2014)
6. M.M. Momeni, Y. Ghayeb, A.A. Mozafari, Optical and photo catalytic characteristics of Ag_2S/TiO_2 nanocomposite films prepared by electrochemical anodizing and SILAR approach. J. Mater. Sci. Mater. Electron. **27**, 11201–11210 (2016)
7. L. Xia, J. Bai, J. Li, Q. Zeng, L. Li, B. Zhou, High-performance $BiVO_4$ photoanodes cocatalyzed with an ultrathin α-Fe_2O_3 layer for photoelectrochemical application. Appl. Catal. B **204**, 127–133 (2017)
8. P.A.K. Reddy, B. Srinivas, V.D. Kumari, M.V. Shankar, M. Subrahmanyam, J.S. Lee, $CaFe_2O_4$ sensitized hierarchical TiO_2 photo composite for hydrogen production under solar light irradiation. Chem. Eng. J. **247**, 152–160 (2014)
9. M.M. Momeni, M. Hakimian, A. Kazempour, Preparation and characterisation of manganese–TiO_2 nanocomposites for solar water splitting. Surf. Eng. **32**, 514–519 (2016)
10. K. Lee, A. Mazare, P. Schmuki, One-dimensional titanium dioxide nanomaterials: nanotubes. Chem. Rev. **114**, 9385–9454 (2014)
11. M.M. Momeni, Y. Ghayeb, Photoelectrochemical water splitting on chromium-doped titanium dioxide nanotube photoanodes prepared by single-step anodizing. J. Alloys Compd. **637**, 393–400 (2015)
12. G.R. Bamwenda, H. Arakawa, The visible light induced photocatalytic activity of tungsten trioxide powders. Appl. Catal. Gen. **210**, 181–191 (2001)
13. A. Martínez-de la Cruz, D.S. Martínez, E.L. Cuéllar, Synthesis and characterization of WO_3 nanoparticles prepared by the precipitation method: evaluation of photocatalytic activity under vis-irradiation. Solid State Sci. **12**, 88–94 (2010)
14. C. Wang, Z. Huang, Controlled synthesis of α-Fe_2O_3 nanostructures for efficient photocatalysis. Mater. Lett. **164**, 194–197 (2016)
15. M.M. Momeni, M. Mahvari, Y. Ghayeb, Photoelectrochemical properties of iron–cobalt $WTiO_2$ nanotube photoanodes for water splitting and photocathodic protection of stainless steel. J. Electroanal. Chem. **832**, 7–23 (2019)
16. M.M. Momeni, Y. Ghayeb, F. Ezati, Fabrication, characterization and photoelectrochemical activity of tungsten–copper co-sensitized TiO_2 nanotube composite photoanodes. J. Colloid Interface Sci. **514**, 70–82 (2018)